

Bidirectional Attention Network for Monocular Depth Estimation

Shubhra Aich*, Jean Marie Uwabeza Vianney*, Md Amirul Islam, Mannat Kaur, and Bingbing Liu†

Abstract—In this paper, we propose a Bidirectional Attention Network (BANet), an end-to-end framework for monocular depth estimation that addresses the limitation of effectively integrating local and global information in convolutional neural networks. The structure of this mechanism derives from a strong conceptual foundation of neural machine translation, and presents a light-weight mechanism for adaptive control of computation similar to the dynamic nature of recurrent neural networks. We introduce bidirectional attention modules that utilize the feed-forward feature maps and incorporate the global context to filter out ambiguity. Extensive experiments reveal the high degree of capability that this bidirectional attention model presents over feed-forward baselines and other state-of-the-art methods for monocular depth estimation on two challenging datasets, KITTI and DIODE. We show that our proposed approach either outperforms or performs at least on a par with the state-of-the-art monocular depth estimation methods with less memory and computational complexity.

I. INTRODUCTION

State-of-the-art methods for depth estimation [1]–[3] are founded on fully convolutional networks (FCN) [4] to estimate the continuous depth map from a single image in an end-to-end manner. Inspired by the success of FCN, recent works on Monocular Depth Estimation (MDE) have shown improvements through higher capacity architectural enhancements to the FCN structure.

Depth perception in human brain requires combined signals from three different cues (oculomotor, monocular, and binocular [5]) to obtain ample information for depth sensing and navigation. As a matter of fact, the domain of MDE is inherently ill-posed. Classical computer vision approaches employ multi-view stereo correspondence algorithms [6], [7] for depth estimation. With the recent deep learning based methods formulate the MDE as a dense, pixel-level, continuous regression problem, although a few approaches attempt to model MDE rather as a classification [8] or quantized regression [1] task.

State-of-the-art MDE models [1]–[3] are based on pre-trained convolutional backbones [9]–[11] with upsampling and skip connection [2], global context module and logarithmic discretization for ordinal regression [1], and coefficient learner for upsampling with local planar assumption [3]. All these design choices explicitly or implicitly suffer from the spatial downsampling operation in the backbone architecture which is shown for pixel-level task [12]. Since MDE is a single plane estimation (i.e., single channel output) problem, in contrast to existing developments for MDE, we incorporate

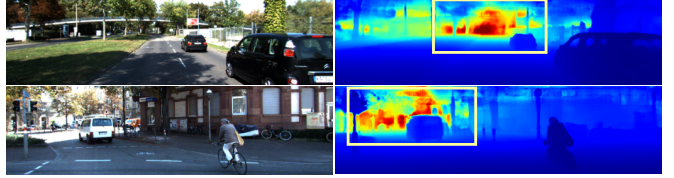


Fig. 1: Examples of BANet predictions on KITTI val set. BANet improves the overall depth estimation by generating attention weights for each stage and diminishing representational ambiguity within the network.

the idea of depth-to-space (D2S) [13], [14] transformation as a remedy to the downsampling operation in the decoding phase. However, straightforward D2S transformation of the final feature map might suffer from the lack of global context from the scene necessary for reliable estimation [15], [16]. Therefore, we inject global context on the D2S transformed single-channel feature maps for each stage of the backbone model. Moreover, we effectively gather the information from all the stages of the backbone with a bidirectional attention module (see Fig. 2) inspired by the work [17] that first demonstrate the potential of attention in deep learning. In the light of the highlighted issues that arise in MDE methods, we present a novel yet effective pipeline for estimating continuous depth map from a single image (see Fig. 1). Although our architecture contains substantially more connections than SOTA, both the computational complexity and the number of parameters are lower than the recent approaches as most of the interactions are computed on D2S transformed single channel features. Due to the prominence of bidirectional attention pattern in our design, we name our model *Bidirectional Attention Network (BANet)*.

Contributions: Our main contributions are as follows:

- To the best of our knowledge we present the first work which applies the concept of bidirectional attention mechanism for monocular depth estimation. The flexibility of our mechanism is its ability to incorporate with any existing CNNs.
- We further introduce *forward* and *backward* attention modules which effectively integrate local and global information to filter out ambiguity.
- We present an extensive set of experimental results on two different MDE datasets. The experiments demonstrate the effectiveness of our proposed method in both the efficiency as well as performance. We show that variants of our proposed mechanism perform better or on a par with the recent SOTA architectures.

*Equal contribution; †corresponding author

Authors are with Noah's Ark Laboratory, Huawei Technologies, Markham, ON L3R5Y1, Canada.

Correspondence: liu.bingbing@huawei.com

II. RELATED WORK

Given the high degree of success of CNNs in image understanding, many methods [1], [2], [8], [18]–[23] have been proposed to tackle the problem of depth estimation.

Supervised MDE. A compiled survey of classical stereo correspondence algorithms for dense disparity estimation is provided in [6]. Saxena *et al.* [18] employed Markov Random Field (MRF) to extract absolute and relative depth magnitudes using the local cues at multiple scales to exploit both local and global information from image patches. Based upon the assumption that the 3D scenes comprise many small planar surfaces (i.e. triangulation), this work is further extended to estimate the 3D position and orientation of the oversegmented superpixels in the images [24], [25].

Eigen *et al.* [26] is the the first work addressing the monocular depth estimation task with deep learning. The authors proposed a stack of global, coarse depth prediction model followed by local region-wise refinement with a separate sub-network. Li *et al.* [27] refined the superpixel depth map predicted by the CNN model to the pixel-level using a CRF. Cao *et al.* [8] transformed the continuous regression task of MDE to the pixel-level classification problem by discretization of depth ranges into multiple bins. A unified approach blending CRF and fully convolutional networks with superpixel pooling for faster inference is proposed into the framework of Deep Convolutional Neural Fields (DCNF) [28]. Multi-scale outputs from different stages of CNN are fused with continuous CRFs in [29] with further refinements via structured attention over the feature maps [19].

Recently, DORN [1] modeled the MDE task as an ordinal regression problem with space-increasing (logarithmic) discretization of the depth range to appropriately address the increase in error with depth magnitude. DenseDepth [2] employed the pretrained DenseNet [11] backbone with bilinear upsampling and skip connections on the decoder to obtain high-resolution depth map. The novelty in the BTS architecture [3] lies in their local planar guidance (LPG) module as an alternative to upsampling based skip connections to transform intermediate feature maps to full-resolution depth predictions. In contrast, we propose a light-weight bidirectional attention mechanism to filter out ambiguity from the deeper representations by incorporating global and local contexts.

Visualization of MDE models: To date, there exist few works [15], [16] on the visualization and possible interpretation of the deep learning models for monocular depth estimation. Hu *et al.* [16] attempted to identify the minimum number of pixels necessary for a trained model to estimate the depth estimator and they showed that CNNs most importantly need the edge pixels to infer the scene geometry and regions surrounding the vanishing points for outdoor scenarios. Dijk and Croon [15] analyzed four pretrained MDE models for interpretability. They found that all the pretrained models considered ignore the apparent size of the objects and focus only on the vertical position of the object in the scene to predict the distance. It means the

models approximate the camera pose while training from the images. This is particularly true for the KITTI dataset for which the camera is mounted on top of the vehicle and the vanishing point of all the scenes is around the middle of the images. Consequently, a small change in pitch corrupt the depth prediction in a non-negligible manner. In our work, we also found both the interpretation of vanishing point and vertical positioning to be quite essential when the training of our models with vertically flipped samples failed to converge.

III. OUR APPROACH

In this section, we discuss our proposed Bidirectional Attention Network (BANet). Specifically, we introduce bidirectional attention modules and different global context aggregation techniques for effective integration of local and global information for the task of monocular depth estimation.

A. Bidirectional Attention Network

The idea of applying bidirectional attention in our proposed approach is motivated by neural machine translation (NMT) [17]. Although there exist recent works [30]–[32] that exploits channel-wise and spatial attention in CNN for various computer vision tasks, the idea of applying attention in forward and backward manner to achieve the nature of bidirectional RNN has not been largely explored.

The overall architecture of our proposed method is illustrated in Fig. 2. Similar to the NMT [17] terminologies, the stage-wise feed-forward features (S_1, S_2, \dots, S_5) in BANet can be seen analogous to the individual word in the source sentence. Note that the bidirectional RNN inherently generates the forward and backward hidden states due to the sequential, dynamic processing of the source sentence word by word. Since CNN has a static nature on the input images, we introduce two different attention modules denoted as forward and backward sub-modules. The bidirectional attention modules take the stage-wise feature maps as input to filter out ambiguity by incorporating global context.

Bidirectional Attention Modules. Since the task of MDE is a single plane estimation problem (i.e., output contains a single channel), we reshape the stage-wise feature maps (s_i where $i = 1, 2, \dots, 5$) to the desired spatial resolution with a 1×1 convolution followed by the efficient and parameterless depth-to-space (D2S) [13], [14] operation. Our forward and backward attention operations can be formalized as:

$$\begin{aligned} s_i^f &= \mathcal{D}_i^f(s_i), \quad a_i^f = \mathcal{A}_i^f(s_1^f, s_2^f, \dots, s_i^f) \\ \mathcal{G}^f &= a_1^f \otimes a_2^f \otimes \dots \otimes a_N^f \\ s_i^b &= \mathcal{D}_i^b(s_i), \quad a_i^b = \mathcal{A}_i^b(s_i^b, s_{i+1}^b, \dots, s_N^b) \\ \mathcal{G}^b &= a_1^b \otimes a_2^b \otimes \dots \otimes a_N^b \\ \mathcal{A} &= \varphi(\mathcal{G}(\mathcal{G}^f \otimes \mathcal{G}^b)) \end{aligned} \quad (1)$$

where $\forall i \in \{1, 2, \dots, N\}$. In Eq. 1, the superscripts \square^f and \square^b denote the operations related to the forward and backward attentions, respectively, and the subscript \square_i denotes the associated stage of the backbone feature maps. \mathcal{D}_i^f and

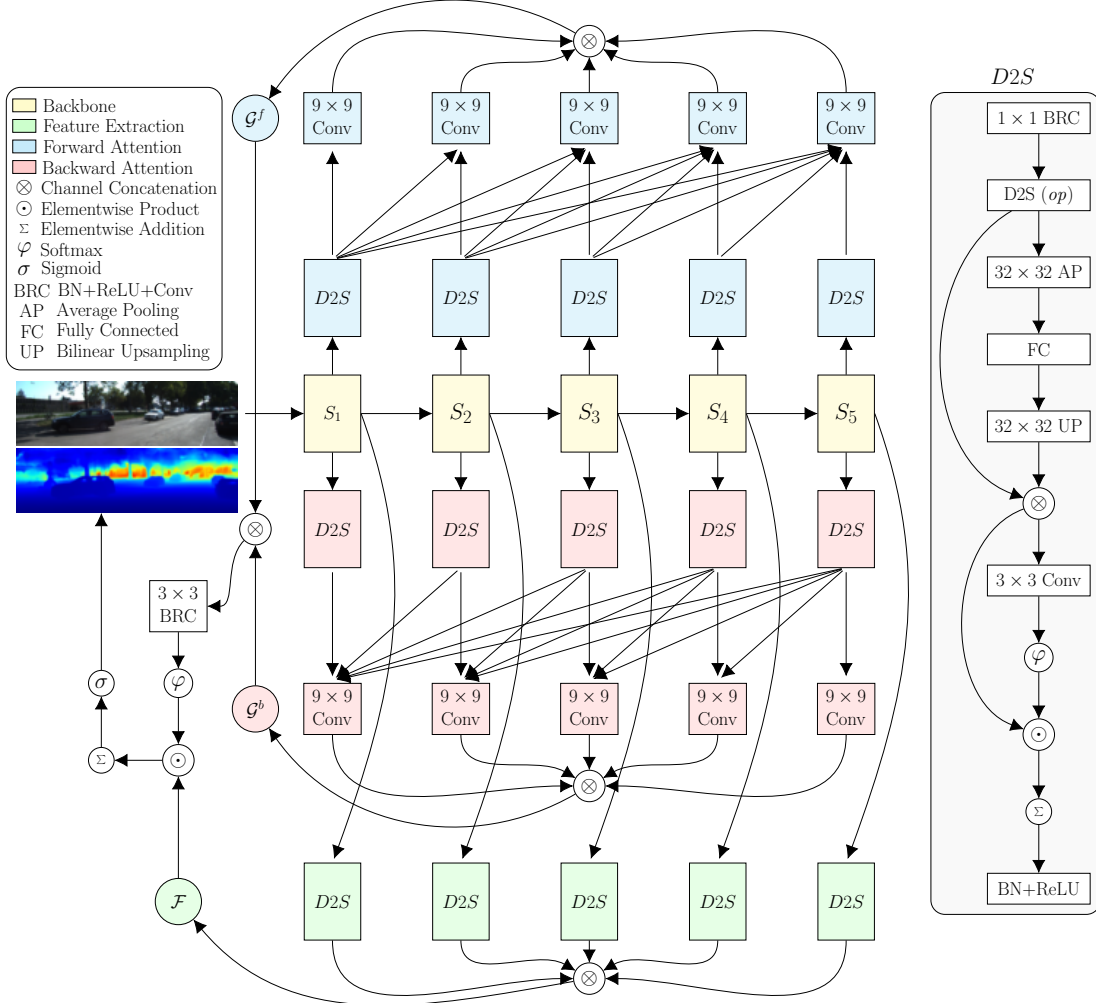


Fig. 2: An architectural illustration of our proposed bidirectional attention network (BANet). The forward and backward attention module take stage-wise features as input and process through multiple operations to generate stage-wise attention weights. The rectangles represent either a single operation or a set of operations with learnable parameters. The white circles with inscribed symbols ($\otimes, \varphi, \odot, \sum, \sigma$) denote parameterless operations. The colored circles highlight the outputs of different conceptual stages of processing. The construction of the $D2S$ modules is shown inside the gray box on the right.

\mathcal{D}_i^b represent the $D2S$ modules which process the backbone feature map s_i . \mathcal{A}_i^f and \mathcal{A}_i^b refers to the 9×9 convolution in Fig. 2. Here, \mathcal{A}_i^f gets access to the features up to the i^{th} stage, and \mathcal{A}_i^b receives the feature representation from the i^{th} stage onward; thus emulating the forward and backward attention mechanisms of a bidirectional RNN. Next, all the forward and backward attention maps are concatenated channel-wise and processed with a 3×3 convolution (\mathcal{G} in Eq. 1) and softmax (φ) to generate the per stage pixel-level attention weights \mathcal{A} (see Fig. 3). The procedure of computing the feature representation, f_i , from the stage-wise feature maps, S_i , using the $D2S$ module can be formalized as:

$$f_i = \mathcal{D}_i^{\mathcal{F}}(s_i); \quad \mathcal{F} = f_1 \otimes f_2 \otimes \dots \otimes f_N \quad (2)$$

where $\forall i \in \{1, 2, \dots, N\}$. Then we compute the unnormalized prediction, \hat{D}_u , from the concatenated features, \mathcal{F} , and attention maps, \mathcal{A} , using the Hadamard (element-wise) product followed by pixel-wise summation \sum . Finally, the

normalized prediction, \hat{D} , is generated with the sigmoid (σ) function. The operations can be expressed as:

$$\hat{D}_u = \sum \mathcal{A} \odot \mathcal{F}, \quad \hat{D} = \sigma(\hat{D}_u) \quad (3)$$

Global Context Aggregation. We incorporate global context inside the $D2S$ modules by applying average pooling with comparatively larger kernels followed by fully connected layers and bilinear upsampling operations. This set of operations combine the pixel-wise, local (query) information with the image-level, global (key) information to extract better monocular cues from the whole image. This aggregation of global context in the $D2S$ module helps to resolve ambiguities (see Fig. 4 and 5) for thinner objects in more challenging scenarios (i.e., very bright or dark contexts). Additionally, we provide details of few alternatives realizations of our proposed architecture as follows:

- **BANet-Full:** This is the complete realization of the architecture as shown in Fig. 2.

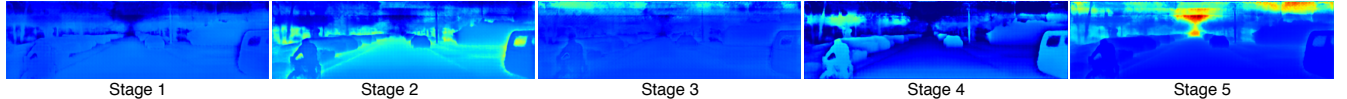


Fig. 3: An illustration of the generated stage-wise attention weights using the forward and backward attention modules.

- **BANet-Vanilla:** It contains only the backbone followed by 1×1 convolution, a single D2S operation, and sigmoid to generate the final depth prediction. This is quite similar to the model used for depth prediction in RefinedMPL [33] for mono 3D detection.
- **BANet-Forward:** The backward attention modules of BANet are missing in this setup.
- **BANet-Backward:** The forward attention modules of BANet are not present here.
- **BANet-Markov:** This follows the Markovian assumption that the feature at each time step (or stage) i depends only on the feature from the immediate preceding (for forward attention) or succeeding (for backward attention) time step (or stage) $i \mp 1$ (i.e. $X_i \perp \{X_{i\mp 2}, X_{i\mp 3}, \dots, X_{i\mp k}\} | X_{i\mp 1}$). Therefore, all but the immediate preceding (forward) and succeeding (backward) incoming edges to the 9×9 convolution in Fig. 2 are deactivated in this construct.
- **BANet-Local:** This one replaces the global context aggregation part with a single 9×9 convolution.

Note that we also conduct pilot experiments without any time dependent structuring by simply concatenating the different stage features all at once and similar post-processing. However, such naive implementation performs much poorer than our proposed time dependent realizations mentioned above. Therefore, we exclude this straightforward employment from further experimental analysis.

IV. EXPERIMENTS

To evaluate the effectiveness of our proposed bidirectional attention framework, we first conduct ablation study with different variants and provide quantitative comparison on two challenging monocular depth estimation dataset (KITTI and DIODE). Next we provide a comparison with recent state-of-the-art methods on KITTI test set.

Datasets. Among several publicly available standard datasets [24], [25], [34]–[36] for monocular depth estimation, we choose DIODE [35] and KITTI [36] due to their comparatively high density of ground truth annotations. We hypothesize that our model assessment might be biased towards better nonlinear interpolator rather than the candidates capable of learning to predict depth maps using monocular cues. Therefore, our experiments done on the datasets comprising truly dense ground truths provide unbiased measure of different types of architectural design choices.

a) DIODE: Dense Indoor/Outdoor DEpth (DIODE) [35] is the first standard dataset for monocular depth estimation comprising diverse indoor and outdoor scenes acquired with the same hardware setup. The training set consists of 8574 indoor and 16884 outdoor samples from 20 scans each. The validation set contains 325 indoor and 446 outdoor samples with each set from 10 different scans. The ground

truth density for the indoor training and validation splits are approximately 99.54% and 99%, respectively. The density of the outdoor sets are naturally lower with 67.19% for training and 78.33% for validation subsets. The indoor and outdoor ranges for the dataset are 50m and 300m, respectively.

b) KITTI: KITTI dataset for monocular depth estimation [36] is a derivative of the KITTI sequences which were designed for autonomous driving. The training, validation, and test sets comprise 85898, 1000, and 500 samples, respectively. Following previous works, we set the prediction range to $[0 - 80m]$ where ever applicable, although there are a few pixels with depth values greater than 80m.

Implementation Details. For fair comparison, we put all the recent models [1]–[3] under the same umbrella by training them from scratch alongside ours using the same hyperparameter settings. All the models are trained for 50 epochs with batch size of 32 in the NVIDIA Tesla V100 32GB GPU using the sparse labels without any densification. The runtime was measured with a single NVIDIA GeForce RTX 2080 Ti GPU just because of its availability at the time of writing. We use Adam optimizer with the initial learning rate of $1e^{-4}$ and weight decay of 0. The learning rate is reduced on plateau after 10 epochs by 0.1 with the minimum learning rate of $1e^{-5}$. Random horizontal flipping and color jitter are the only augmentation strategies used in training. For KITTI, we randomly crop 352×1216 training samples following the resolution of the validation and test splits. Also, for computational efficiency, the inputs are half-sampled (and zero-padded if necessary) prior to feeding into the models, and the predictions are bilinearly upsampled to match the ground truth before comparison. For DORN [1], we set the number of ordinal levels to the optimal value of 80 (or 160 considering both positive and negative planes). This value is set to 50, 75, and 75 for DIODE indoor, outdoor, and combined splits following the same principle. We employ SILog and \mathcal{L}_1 error as the loss functions for training all the models on KITTI and DIODE, respectively, except for DORN that comes with its own ordinal loss. Following BTS [3] and DenseDepth [2], we use DenseNet161 [11] as our BANet backbone.

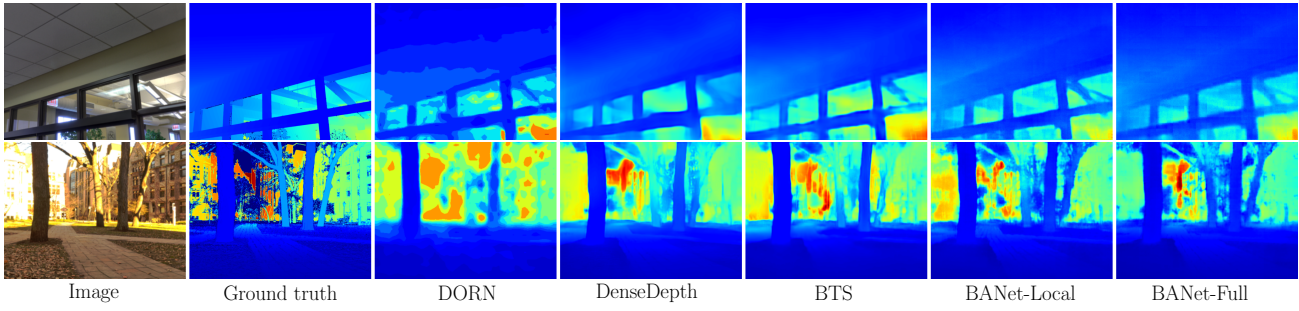
Evaluation Metrics. In MDE literature, both accuracy (higher is better) and error (lower is better) metrics are used altogether to benchmark different approaches. However, there is a lack of consistency among the set of metrics used for different datasets. In this work, we employ a unified set of metrics across all the subsets of different datasets used for experiments. For the error metrics, we mostly follow the measures (SILog, SqRel, AbsRel, MAE, RMSE, iRMSE) directly from the KITTI leadearboard. Additionally, we have modified the accuracy metrics for more rigorous measurements since the traditional accuracy metrics are thresholded measures of relative predictions over an interval. We extend

TABLE I: Quantitative results on the **DIODE Indoor** *val* set.

Model	#Params (10 ⁶)	Time (ms)	Lower is better						Higher is better (%)					
			SiLog	SqRel	AbsRel	MAE	RMSE	iRMSE	δ ₅	δ ₁₀	δ ₁₅	δ ₂₅	δ ₅₆	δ ₉₅
DORN [1]	91.21	57	23.94	44.00	45.15	1.65	1.88	206.38	9.58	18.00	25.47	38.15	62.25	76.98
DenseDepth [2]	44.61	27	19.67	25.10	34.50	1.39	1.56	177.33	12.37	23.75	33.28	48.13	70.19	83.00
BTS [3]	47.00	34	19.27	24.23	32.93	1.41	1.59	174.34	14.40	26.83	36.85	50.66	71.87	82.00
BANet-Vanilla	28.73	21	18.78	27.75	34.36	1.43	1.61	175.35	14.13	26.43	36.43	51.28	70.63	81.32
BANet-Forward	32.58	28	18.39	25.81	35.49	1.49	1.65	179.58	12.63	24.29	33.76	47.53	68.63	80.91
BANet-Backward	32.58	28	18.25	24.43	34.19	1.46	1.62	176.02	13.58	25.05	34.93	48.94	69.50	81.52
BANet-Markov	35.64	31	18.62	21.78	32.58	1.44	1.61	173.58	12.79	24.39	34.60	48.99	72.28	82.29
BANet-Local	35.08	32	18.83	23.65	33.49	1.43	1.59	172.11	13.53	25.53	35.11	49.71	71.18	82.88
BANet-Full	35.64	33	18.43	26.49	34.99	1.45	1.61	177.22	13.15	24.34	33.56	48.48	70.66	82.26

TABLE II: Quantitative results on the **DIODE Outdoor** *val* set.

Model	#Params (10 ⁶)	Time (ms)	Lower is better						Higher is better (%)					
			SiLog	SqRel	AbsRel	MAE	RMSE	iRMSE	δ ₅	δ ₁₀	δ ₁₅	δ ₂₅	δ ₅₆	δ ₉₅
DORN [1]	91.31	57	41.11	382.60	56.17	5.81	8.88	97.84	10.79	21.07	30.81	46.72	74.69	86.42
DenseDepth [2]	44.61	27	37.49	244.47	41.74	4.32	7.03	110.19	16.87	30.75	41.99	58.56	81.14	90.05
BTS [3]	47.00	34	38.11	254.55	44.97	4.57	7.36	94.93	14.01	26.71	37.49	54.71	79.92	89.35
BANet-Vanilla	28.73	21	37.38	217.52	39.53	4.19	6.93	92.85	16.32	30.72	42.04	58.95	81.42	90.09
BANet-Forward	32.58	28	37.59	202.70	38.80	4.25	7.00	93.40	16.14	30.13	41.75	58.46	80.81	89.72
BANet-Backward	32.58	28	36.89	215.27	39.15	4.21	6.86	92.44	15.70	29.83	41.35	57.89	81.34	90.37
BANet-Markov	35.64	31	37.61	226.07	39.86	4.27	6.97	92.86	16.09	30.21	42.00	58.46	81.24	90.00
BANet-Local	35.08	32	36.54	218.54	39.23	4.11	6.78	92.72	16.26	30.44	42.26	59.68	82.35	90.56
BANet-Full	35.64	33	37.17	210.97	38.50	4.20	6.94	92.26	16.87	31.25	42.81	58.66	81.53	90.33

Fig. 4: Sample results on DIODE indoor (top) and outdoor (bottom) images. **Top:** The window frame on the bottom right is detected well by BANets compared to BTS and DenseDepth. **Bottom:** Other methods but our BANet-Full fail to localize the highly illuminated tree trunks. This shows the importance of global context aggregation in BANet-Full.

this set placing more thresholds between the lower end and the lowest existing threshold within the same interval (Eq. 4).

$$\delta_k = \sum_i \max\left(\frac{a_i t_i}{t_i a_i}\right) < \left(1 + \frac{k}{100}\right) * 100 \text{ (%) } (4)$$

where $k \in \{5, 10, 15, 25, 56, 95\}$. Consequently, our extended set contains six metrics (*i.e.* δ_5 , δ_{10} , δ_{15} , δ_{25} , δ_{56} , and δ_{95}), of which the last three represent the old metrics (δ_1^{old} , δ_{10}^{old} , δ_3^{old}). Such a more rigorous metric extension provides better insights for autonomous driving applications, where the high precision of depth estimation is of paramount importance [33].

A. Results on Monocular Depth Estimation

Quantitative Comparison: Table I, II, III, and IV list the comparison results of our BANet variants with the SOTA architectures. Note that the performance of DORN is particularly much worse than others due the effect of granularity provided by its discretization or ordinal levels. Setting up a higher value for this hyperparameter might improve its

precision. However, increasing this number causes exponential increase in memory consumption during training; thus making it difficult to train on large datasets like KITTI and DIODE. Overall, our BANet variants performs better or close to existing SOTA in particular BTS. It is worth noting that the number of parameters in the heaviest BANet variant (BANet-Full) is about 25% less than BTS.

To better tease out the effect of the different components in BANet, we provide observations as follows:

- BANet-Markov performs worse than BANet-Local and BANet-Full where both of these realizations include all the forward and backward edges in Figure 2. It shows that the Markovian assumption does not hold well among different stages of a convolutional network.
- The superior performance of BANet-Backward compared to BANet-Forward indicates that the feature refinement is possibly more important in the early stages of the backbone than later in terms of performance.
- The time dependent structure inscribed into the model improves the performance over the vanilla counterparts with little increase in computational and memory complexity.

TABLE III: Quantitative results on the **DIODE All** (Indoor+Outdoor) *val* set.

Model	#Params (10 ⁶)	Time (ms)	Lower is better						Higher is better (%)					
			SiLog	SqRel	AbsRel	MAE	RMSE	iRMSE	δ_5	δ_{10}	δ_{15}	δ_{25}	δ_{56}	δ_{95}
DORN [1]	91.31	57	34.14	218.36	45.74	3.58	5.39	132.58	11.91	22.62	32.42	48.05	74.58	86.79
DenseDepth [2]	44.61	27	31.05	157.70	39.33	3.10	4.77	182.26	15.26	28.28	38.80	54.25	76.46	87.24
BTS [3]	47.00	34	30.06	128.67	37.03	3.13	4.83	142.98	15.85	29.31	40.00	54.98	76.18	86.52
BANet-Vanilla	28.73	21	30.11	156.16	39.30	3.08	4.73	129.02	14.61	27.30	37.90	53.76	76.67	87.37
BANet-Forward	32.58	28	30.54	181.53	39.09	3.05	4.77	128.88	15.34	28.69	39.65	55.17	76.86	87.21
BANet-Backward	32.58	28	30.28	179.41	40.25	3.05	4.73	129.98	15.27	27.96	38.42	54.17	76.83	87.47
BANet-Markov	35.64	31	30.16	188.45	40.10	3.12	4.80	129.31	15.20	27.89	38.35	54.04	76.04	86.76
BANet-Local	35.08	32	29.69	148.91	37.68	2.98	4.66	126.96	16.03	29.44	40.36	56.08	77.34	87.96
BANet-Full	35.64	33	29.93	150.76	39.28	3.06	4.73	130.39	14.48	26.85	37.10	53.26	76.40	87.15

TABLE IV: Quantitative results on the **KITTI** *val* set.

Model	#Params (10 ⁶)	Time (ms)	Lower is better						Higher is better (%)					
			SiLog	SqRel	AbsRel	MAE	RMSE	iRMSE	δ_5	δ_{10}	δ_{15}	δ_{25}	δ_{56}	δ_{95}
DORN [1]	89.23	36	12.22	3.03	11.78	2.04	3.80	11.68	27.63	53.10	73.55	91.28	98.45	99.53
DenseDepth [2]	44.61	25	10.66	1.76	8.01	1.58	3.31	8.24	49.88	74.38	84.81	93.50	98.87	99.69
BTS [3]	47.00	29	10.67	1.59	7.51	1.56	3.37	8.10	52.83	75.57	85.51	93.80	98.71	99.65
BANet-Vanilla	28.73	20	10.88	1.65	7.74	1.63	3.51	8.34	49.61	74.04	84.68	93.49	98.63	99.59
BANet-Forward	32.34	25	10.61	1.67	9.02	1.77	3.54	9.99	33.31	65.93	81.36	92.66	98.68	99.61
BANet-Backward	32.34	25	10.54	1.52	7.67	1.59	3.42	8.47	49.41	73.99	84.95	93.57	98.72	99.65
BANet-Markov	35.28	27	10.72	1.85	8.24	1.62	3.38	8.28	48.34	74.37	84.87	93.19	98.75	99.69
BANet-Local	35.08	27	10.53	2.21	9.92	1.77	3.34	9.68	33.41	66.61	81.74	92.36	98.87	99.71
BANet-Full	35.28	28	10.64	1.81	8.25	1.60	3.30	8.47	45.73	74.19	85.45	93.75	98.81	99.68

- The advantage of global context aggregation is not numerically well-understood from the tables. However, from Fig. 4 and 5, it is an evident that exploiting the global information helps to disambiguate in delicate situations.

TABLE V: Results on the KITTI leaderboard (test set).

Method	SiLog	SqRel	AbsRel	iRMSE
DORN [1]	11.77	2.23	8.78	12.98
BTS [3]	11.67	2.21	9.04	12.23
BANet-Full	11.61	2.29	9.38	12.23

Finally, we also compare our BANet-Full with other methods on the KITTI leaderboard (Table V). Our model achieves slightly better than SOTA architectures on the primary metric (SiLog) used for ranking.

Qualitative Comparison: Figure 4 and 5 show the qualitative comparison of different SOTA methods. The DORN prediction map clearly indicates its semi-discretized nature of prediction. For both the indoor and outdoor images in Fig. 4, BTS and DenseDepth suffer from the high intensity regions surrounding the window frame in the bottom right of the left image and the trunks in the right image. Our BANet variants work better in these delicate regions. In particular, the global context aggregation of BANet-Full helps to distinguish the trunks better than its local counterpart. Fig. 5 demonstrates a similar case, but this time in the dark surroundings. From both these visualizations, it is evident that the global context aggregation is necessary to resolve potential ambiguities caused by adverse illumination.

V. CONCLUSION

In this paper, we have presented a bidirectional attention mechanism for convolutional networks for monocular depth estimation task similar to bidirection RNN for NMT. We show that a standard backbone equipped with this attention

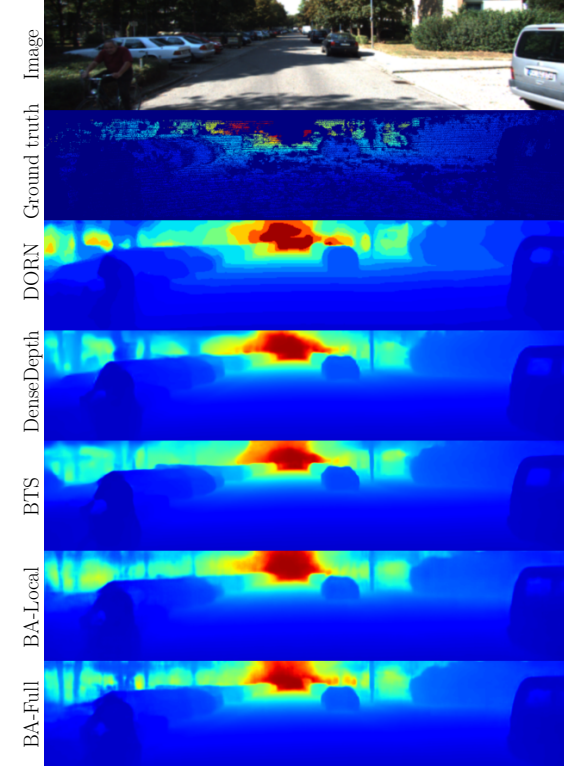


Fig. 5: Sample results on KITTI *val* set. The top region is cropped since it does not contain any ground truth. The tree trunks in the dark regions on the left is better differentiated with global context aggregation in BANet-Full.

mechanism performs better or at least on a par with the SOTA architectures on standard datasets. As a future direction, we believe that our proposed attention mechanism has the potential to be useful in similar dense prediction tasks, e.g., the single plane ones.

REFERENCES

[1] H. Fu, M. Gong, C. Wang, K. Batmanghelich, and D. Tao, “Deep ordinal regression network for monocular depth estimation,” in *CVPR*, 2018. 1, 2, 4, 5, 6

[2] I. Alhashim and P. Wonka, “High quality monocular depth estimation via transfer learning,” *CoRR*, vol. abs/1812.11941, 2018. 1, 2, 4, 5, 6

[3] J. H. Lee, M. Han, D. W. Ko, and I. H. Suh, “From big to small: Multi-scale local planar guidance for monocular depth estimation,” *CoRR*, vol. abs/1907.10326, 2019. 1, 2, 4, 5, 6

[4] J. Long, E. Shelhamer, and T. Darrell, “Fully convolutional networks for semantic segmentation,” in *CVPR*, 2015. 1

[5] E. Goldstein, *Sensation and Perception*. Cengage Learning, 2009. 1

[6] D. Scharstein and R. Szeliski, “A taxonomy and evaluation of dense two-frame stereo correspondence algorithms,” *IJCV*, vol. 47, 2002. 1, 2

[7] S. M. Seitz, B. Curless, J. Diebel, D. Scharstein, and R. Szeliski, “A comparison and evaluation of multi-view stereo reconstruction algorithms,” in *CVPR*, 2006. 1

[8] Y. Cao, Z. Wu, and C. Shen, “Estimating depth from monocular images as classification using deep fully convolutional residual networks,” *IEEE Transactions on Circuits and Systems for Video Technology*, vol. 28, no. 11, 2018. 1, 2

[9] K. Simonyan and A. Zisserman, “Very deep convolutional networks for large-scale image recognition,” in *ICLR*, 2015. 1

[10] K. He, X. Zhang, S. Ren, and J. Sun, “Deep residual learning for image recognition,” in *CVPR*, 2016. 1

[11] G. Huang, Z. Liu, L. Van Der Maaten, and K. Q. Weinberger, “Densely connected convolutional networks,” in *CVPR*, 2017. 1, 2, 4

[12] M. Amirul Islam, M. Rochan, N. D. Bruce, and Y. Wang, “Gated feedback refinement network for dense image labeling,” in *CVPR*, 2017. 1

[13] W. Shi, J. Caballero, F. Huszar, J. Totz, A. P. Aitken, R. Bishop, D. Rueckert, and Z. Wang, “Real-time single image and video super-resolution using an efficient sub-pixel convolutional neural network,” in *CVPR*, 2016. 1, 2

[14] S. Aich, W. van der Kamp, and I. Stavness, “Semantic binary segmentation using convolutional networks without decoders,” in *CVPRW*, 2018. 1, 2

[15] T. v. Dijk and G. d. Croon, “How do neural networks see depth in single images?” in *ICCV*, 2019. 1, 2

[16] J. Hu, Y. Zhang, and T. Okatani, “Visualization of convolutional neural networks for monocular depth estimation,” in *ICCV*, 2019. 1, 2

[17] D. Bahdanau, K. Cho, and Y. Bengio, “Neural machine translation by jointly learning to align and translate,” in *ICLR*, 2015. 1, 2

[18] A. Saxena, S. H. Chung, and A. Y. Ng, “Learning depth from single monocular images,” in *NIPS*, 2006. 2

[19] D. Xu, W. Wang, H. Tang, H. Liu, N. Sebe, and E. Ricci, “Structured attention guided convolutional neural fields for monocular depth estimation,” in *CVPR*, 2018. 2

[20] Y. Gan, X. Xu, W. Sun, and L. Lin, “Monocular depth estimation with affinity, vertical pooling, and label enhancement,” in *ECCV*, 2018. 2

[21] A. Roy and S. Todorovic, “Monocular depth estimation using neural regression forest,” in *CVPR*, 2016. 2

[22] J.-H. Lee and C.-S. Kim, “Monocular depth estimation using relative depth maps,” in *CVPR*, 2019. 2

[23] J. Chang and G. Wetzstein, “Deep optics for monocular depth estimation and 3d object detection,” in *ICCV*, 2019. 2

[24] A. Saxena, S. H. Chung, and A. Y. Ng, “Learning depth from single monocular images,” in *NIPS*, 2006. 2, 4

[25] A. Saxena, M. Sun, and A. Y. Ng, “Make3d: Learning 3d scene structure from a single still image,” *IEEE Transactions on Pattern Analysis and Machine Intelligence*, vol. 31, no. 5, pp. 824–840, 2009. 2, 4

[26] D. Eigen, C. Puhrsch, and R. Fergus, “Depth map prediction from a single image using a multi-scale deep network,” in *NIPS*, 2014. 2

[27] B. Li, C. Shen, Y. Dai, A. van den Hengel, and M. He, “Depth and surface normal estimation from monocular images using regression on deep features and hierarchical crfs,” in *CVPR*, 2015. 2

[28] F. Liu, C. Shen, G. Lin, and I. Reid, “Learning depth from single monocular images using deep convolutional neural fields,” *IEEE TPAMI*, vol. 38, no. 10, 2016. 2

[29] D. Xu, E. Ricci, W. Ouyang, X. Wang, and N. Sebe, “Multi-scale continuous crfs as sequential deep networks for monocular depth estimation,” in *CVPR*, 2017. 2

[30] J. Hu, L. Shen, and G. Sun, “Squeeze-and-excitation networks,” in *CVPR*, 2018. 2

[31] S. Woo, J. Park, J.-Y. Lee, and I. S. Kweon, “Cbam: Convolutional block attention module,” in *ECCV*, 2018. 2

[32] H. Zhang, K. Dana, J. Shi, Z. Zhang, X. Wang, A. Tyagi, and A. Agrawal, “Context encoding for semantic segmentation,” in *CVPR*, 2018. 2

[33] J. M. U. Vianney, S. Aich, and B. Liu, “Refinedmpl: Refined monocular pseudolidar for 3d object detection in autonomous driving,” 2019. 4, 5

[34] N. Silberman, D. Hoiem, P. Kohli, and R. Fergus, “Indoor segmentation and support inference from rgbd images,” in *ECCV*, 2012. 4

[35] I. Vasiljevic, N. Kolkin, S. Zhang, R. Luo, H. Wang, F. Z. Dai, A. F. Daniele, M. Mostajabi, S. Basart, M. R. Walter, and G. Shakhnarovich, “DIODE: A Dense Indoor and Outdoor DEpth Dataset,” *CoRR*, vol. abs/1908.00463, 2019. 4

[36] J. Uhrig, N. Schneider, L. Schneider, U. Franke, T. Brox, and A. Geiger, “Sparsity invariant cnns,” in *3DV*, 2017. 4